Validating simple dynamical simulations of the unitary Fermi gas

Michael McNeil Forbes[1,2,3,*] and Rishi Sharma[4,5,†]

[1]*Institute for Nuclear Theory, University of Washington, Seattle, Washington 98195-1550, USA*

[2]*Department of Physics, University of Washington, Seattle, Washington 98195-1560, USA*

[3]*Department of Physics and Astronomy, Washington State University, Pullman, Washington 99164-2814, USA*

[4]*TRIUMF, Vancouver, British Columbia V6T 2A3, Canada*

[5]*Department of Theoretical Physics, Tata Institute of Fundamental Research, Homi Bhabha Road, Mumbai 400005, India*

(Received 26 August 2013; published 31 October 2014)

We present a comparison between simulated dynamics of the unitary fermion gas using the superfluid local density approximation (SLDA) and a simplified bosonic model, the extended Thomas-Fermi (ETF) with a unitary equation of state. Small-amplitude fluctuations have similar dynamics in both theories for frequencies far below the pair-breaking threshold and wave vectors much smaller than the Fermi momentum. The low-frequency linear responses in both match well for surprisingly large wave vectors, even up to the Fermi momentum. For nonlinear dynamics such as vortex generation, the ETF provides a semiquantitative description of SLDA dynamics as long as the fluctuations do not have significant power near the pair-breaking threshold; otherwise the dynamics of the ETF cannot be trusted. Nonlinearities in the ETF tend to generate high-frequency fluctuations, and with no normal component to remove this energy from the superfluid, features such as vortex lattices cannot relax and crystallize as they do in the SLDA.

DOI: 10.1103/PhysRevA.90.043638 PACS number(s): 67.85.−d, 71.15.Mb, 31.15.E−, 03.75.Hh

The motion of cold Fermi superfluids under dynamical stimuli has been of interest to a variety of research fields. A classic example is the discovery of the Josephson effect [1] in superconductors. Now it is possible to track the motion of magnetic vortices in real time [2–5], and to ramp the fermionic interaction in cold-atom experiments from the Bardeen-Cooper-Schrieffer (BCS) to the Bose-Einstein condensate (BEC) regimes [6]. Furthermore, by changing the trapping potential, phenomena such as particle transport [7,8] and cloud collision dynamics [9] have been quantitatively measured. More recently, "heavy solitons" were observed oscillating in elongated traps [10] with very long periods. Many nuclear responses [11] and reaction processes [12] are manifestations of collective dynamics of nucleons, and vortex pinning and unpinning likely plays a role in generating glitches in the spin down of neutron stars [13].

Despite this diverse interest, simulating fermionic quantum hydrodynamics—even with simplified time-dependent density functional theory (DFT) models—remains a computational challenge, requiring world-class computing resources for even relatively simple problems [14]. Direct simulation of many macroscopic phenomena lies outside the realm of current technology, so in this paper, we validate to what extent a computationally simple model called the extended Thomas-Fermi (ETF) model can characterize the dynamics of the strongly interacting unitary Fermi gas (UFG). We find that it performs well for low-frequency dynamics, and identify its limitations. This validation played a crucial role in solving the mystery of the "heavy solitons" observed in [10] where the ETF was used to demonstrate the consistency of the observations with vortex rings instead of solitons [15].

The computational problem is that most fermionic superfluid DFTs [of the Kohn-Sham variety such as the Bogoliubov–de Gennes (BdG) mean-field equations or Hartree-Fock-Bogoliubov (HFB) equations] require evolving hundreds of thousands of single-particle wave functions, occupying vast amounts of memory. In contrast, the Gross-Pitaevskii equation (GPE) [16,17] provides an attractive computational method for studying bosonic superfluids where the superfluid is represented by a single wave function for the condensed state. The ETF model considered here has the same computational simplicity, and thus can be applied to macroscopic systems. We find that it performs well for low-frequency dynamics, suggesting that it might provide the basis for a practical method of simulating macroscopic volumes of fermionic superfluids required to understand phenomena such as neutron star glitches.

The UFG is a universal model for dilute Fermi gases comprising two species of the same mass interacting with a zero-range resonant attractive interaction of infinite s-wave scattering length. It provides an ideal problem to benchmark many-body techniques for several reasons: it has a simple and universal equation of state (EOS) but remains highly nonperturbative with strong interactions, is directly realized in cold-atom experiments [18], and provides a good approximation for the dilute neutron matter [19] in the crusts of neutron stars. This universal system is stable, and the absence of a length scale for the interaction implies that the energy-density $\mathcal{E}(\rho) = \xi\mathcal{E}_{FG}(\rho)$ is characterized by the single universal dimensionless coefficient ξ known as the Bertsch parameter [20]. [Here $\mathcal{E}_{FG}(\rho) = \frac{3}{5}\rho E_F(\rho)$ is the energy density of the noninteracting system with total density $\rho = \rho_a + \rho_b = k_F^3/3\pi^2$, $E_F(\rho) = \hbar^2k_F^2/2m$ is the Fermi energy, and k_F is the Fermi wave vector.] Despite the simple form of the EOS, the system is strongly interacting and admits no perturbative expansions. Significant effort has been put into determining the Bertsch parameter ξ over the past decade, and only recently has it been computed [21–25], and measured [26–28] to high precision (see [29] for a survey). The current best-fit value $\xi = 0.3742(5)$ is obtained by consistently fitting both quantum Monte Carlo (QMC) and

*mforbes@alum.mit.edu

†rishi@theory.tifr.res.in

experimental results [25] with a self-consistent fermionic DFT called the superfluid local density approximation (SLDA).

The time-dependent generalization of the SLDA provides a model for directly studying time-dependent phenomena in the UFG (see [30] for a review). The SLDA includes pair-breaking effects, the superfluid-normal transition, and finite-size (shell) effects. Many different dynamical processes have been described in [14], including vortex nucleation through stirring, vortex-vortex interactions, and vortex ring formation. These simulations, however, required supercomputing resources for even modest physical volumes. The largest system studied in [14] contained ∼500 particles represented by 70 000 wave functions on a $32 \times 32 \times 192$ lattice. To compare, typical cold-atom experiments comprise some 10^5 particles [31], which would severely tax current computational resources, even if symmetries are utilized. Similarly, while the dynamics of a single vortex in neutron matter may be within reach of cutting edge computing [32], simulating multiple vortices separated by several lattice lengths will require significantly more resources. Thus, validating and generalizing computationally more efficient methods such as the ETF model is critical for scaling calculations up to macroscopic systems.

The ETF [33–35] is essentially a bosonic theory describing dimers or Cooper pairs in the UFG with a single collective condensate wave function that has been used to analyze the expansion and breathing mode frequencies of cold-atomic gases in a trap [33,36,37], their surface oscillations [38], collisions of clouds of fermions [39], vortex generation [40], vortex pinning [32], instabilities [41], and soliton dynamics [42]. While the ETF has the same symmetries, and can be tuned to have the same EOS as the full theory, one expects poor behavior when excitations approach the pair-breaking threshold set by the gap $\hbar\omega > 2\Delta \approx E_F$. The only low-energy degree of freedom—the superfluid phonon—exists in both theories, and matching the EOSs ensures that the speed of sound is the same. This ensures that the linear response for small frequencies and momenta match, but we find good agreement for small frequencies even at finite momenta $q \sim k_F$, suggesting that the ETF could be a good description of SLDA dynamics for slowly varying probes. Indeed, the ETF seems to do a good job of describing bulk dynamics in regimes where pair-breaking effects play a minor role, but exhibits notable departures as one introduces excitations near the pair-breaking threshold. We verify this behavior by comparing with existing fermionic [14] simulations and find certain diagnostics to check whether the bosonic simulation can be expected to be a good description of the fermionic problem.

Indeed, we find qualitative differences between ETF and SLDA simulations when we produce excitations with frequencies higher than the pair-breaking threshold and wave vectors larger than the inverse particle separation. One way to remove these high-wave-vector components in the ETF is to average the order parameter over a region of size of the order of the particle separation. This reduces the average amplitude of the order parameter, an effect that is also seen in the SLDA. This motivates us to compare the evolution of a integral of the square of the order parameters (scaled so that the dimensions are appropriate) in the two theories. If the integral does not change significantly as a function of time we can expect the ETF to be a reasonable description of the SLDA evolution. This criterion should be seen as a quick heuristic check: a more concrete analysis involves calculating the full spectrum of fluctuations to check whether modes with frequencies above 2Δ and wave vectors greater than k_F are occupied.

In Secs. I and II we review the SLDA and the ETF models. We compare the linear response for time-independent fluctuations in Sec. III and for dynamic fluctuations in Sec. IV. In Sec. V we compare the ETF with SLDA dynamics for a family of simulations where vortices are created and nonlinear effects are important, and conclude in Sec. VI. We present a discussion of the numerical implementation in Appendix A and give some details of the simulation parameters in Appendix B.

I. THE SLDA

We start with a brief review of the SLDA DFT. Density functional theory (DFT) is in principle an exact approach, widely used in nuclear physics (see [43] for a review) and in quantum chemistry to describe normal (i.e., non-superfluid) systems. It provides a framework capable of assimilating *ab initio* and experimental results into a computationally tractable and predictive framework. The original Hohenberg-Kohn formulation [44] proves the existence of an energy functional $E[\rho(x)]$ such that the density $\rho_0(x)$ and energy E_0 of the ground state of an interacting system in an external potential $V(x)$ can be found by minimizing

$$E_0 = \min_{\rho(x)} \left(E_{\text{DFT}}[\rho(x)] + \int d^3x \; V(x)\rho(x) \right). \tag{1}$$

Dynamics may be described by an extension commonly referred to as the time-dependent density functional theory (we will refer to it as DFT as well) [45] that describes the evolution of the one-body number density in the presence of an arbitrary one-body external field. As in the static case one can prove the existence of a functional from which one can determine the exact time-dependent number density for a given quantum system [45]. Unfortunately, these theorems do not specify the form of the functional $E_{\text{DFT}}[\rho(x)]$.

Instead, one must rely on physically motivated models and benchmark them. To model the UFG, a simple form known as the superfluid local density approximation (SLDA) [46] has been successfully benchmarked against *ab initio* QMC calculations [25]. It is a local functional of the density ρ and two additional densities: a kinetic density $\tau(x) \propto \langle \nabla\psi^\dagger \cdot \nabla\psi \rangle$ (following the Kohn-Sham formulation [47]) which is required to model finite-size (shell) effects, and an anomalous density $\nu \propto \langle \psi\psi \rangle$ required to model pairing effects (see [25,30,48] for a discussion). The resulting SLDA energy density functional

$$\begin{aligned} \mathcal{E}_{\text{SLDA}} &= \frac{\hbar^2}{m}\left(\frac{\alpha}{2}\tau + g\nu^\dagger\nu\right) + \beta\mathcal{E}_{FG}(\rho) \\ g^{-1} &= \frac{\rho^{1/3}}{\gamma} - \frac{k_c}{2\pi\alpha} \end{aligned} \tag{2}$$

has three dimensionless parameters: an inverse effective mass α (that multiplies the kinetic density τ), a self-energy β, and a pairing parameter γ. (The anomalous density ν diverges in the local approximation requiring regulation expressed through a cutoff $k_c \to \infty$.) One typically solves the SLDA

for homogeneous matter, expressing β and γ in terms of the physically relevant Bertsch parameter ξ and the $T = 0$ pairing gap $\eta = \Delta/E_F$. If the effective mass parameter $\alpha \neq 1$, then one must also introduce a term involving currents to restore Galilean covariance that slightly complicates the numerical implementation. For this reason, and since $\alpha \approx 1$, the SLDA employed in practice typically sets $\alpha = 1$ [14] and we shall compare to these results in this paper.

To work with this DFT, one expresses τ, ρ, and ν in terms of a set of single-particle orbitals that obey a set of self-consistency equations similar to the BdG mean-field equations

$$i\hbar\frac{\partial}{\partial t}\begin{pmatrix}u_n(x,t)\\ v_n(x,t)\end{pmatrix} = \begin{pmatrix}\hat{K}+U & \Delta\\ -\Delta^* & -\hat{K}-U\end{pmatrix}\begin{pmatrix}u_n(x,t)\\ v_n(x,t)\end{pmatrix}, \quad (3)$$

where $U[\tau,\rho,\nu]$ and $\Delta[\tau,\rho,\nu]$ are functions of the densities obtained by minimizing (2). The computational difficulty is that one must simultaneously evolve many single-particle wave functions, (u_n, v_n), and one eventually becomes limited by memory (70 000 wave functions on a $32 \times 32 \times 192$ grid requires 200 GB for a single step).

We note that the SLDA reproduces the variational BdG mean-field equations if one sets the effective mass to unity $\alpha = 1$, removes the self-energy $\beta = 0$, and tunes the pairing interaction with the usual pseudopotential $\gamma^{-1} = 0$. This well-studied approximation captures the same qualitative physics as the SLDA, but does not provide a reliable quantitative picture (the lack of a self-energy $\beta = 0$ for example incorrectly predicts a noninteracting polaron with zero binding energy). The SLDA will reproduce this model if one fixes the parameters $\alpha = 1$, $\xi = 0.5906\cdots$, and $\eta = 0.6864\cdots$. Since this BdG model has been widely studied, we include a comparison between it and the ETF tuned to this "incorrect" value of ξ along with the comparison to the SLDA.

II. THE ETF MODEL

In contrast, the Gross-Pitaevskii equation (GPE) [16,17] commonly used to model bosonic superfluids requires storing and evolving only a single complex wave function ψ representing the condensate, thereby allowing one to explore significantly larger systems. To apply this approach to the UFG we note that one can describe the BEC limit of strong attraction as a Bose gas of dimers. Hence, we introduce $\Psi(x,t)$ as the collective dimer wave function into a modified GPE [34,35]:

$$E_{\rm ETF}[\Psi] = \int d^3x\left(\frac{\hbar^2|\nabla\Psi(x)|^2}{4m} + V(x)\rho + g(\rho) - \frac{\hbar^2(1-4\lambda)}{32m}\frac{(\nabla\rho)^2}{\rho}\right), \quad (4a)$$

$$\frac{i\hbar\partial_t\Psi}{2} = \mathbf{H}\Psi = \left(-\frac{\hbar^2\nabla^2}{8m} + V + g'(\rho) + \frac{\hbar^2(1-4\lambda)}{8m}\frac{\nabla^2\sqrt{\rho}}{\sqrt{\rho}}\right)\Psi, \quad (4b)$$

$$\rho = 2|\Psi|^2, g(\rho) = \xi\mathcal{E}_{FG}(\rho), g'(\rho) = \xi E_F(\rho). \quad (4c)$$

The form of the coefficient of the term $(\nabla\rho)^2/\rho$ in Eq. (4a) has been chosen so that in the absence of phase fluctuations one gets back the form adopted in Ref. [35].

One should think of this as a GPE for the "dimer" Cooper pairs. The bosonic dimers are described by the collective wave function $\Psi(x,t)$ with the interpretation that $|\Psi|^2$ is the dimer density; hence the total density $\rho = 2|\Psi|^2$ has a factor of 2. Likewise, the bosonic mass $m_B = 2m$ is twice the fermionic mass, accounting for the factor of $4m = 2m_B$ in the kinetic term. This picture becomes more accurate as the dimers become more tightly bound toward the BEC regime where a GPE description of the bosonic dimers is applicable. Finally, whereas the GPE has a quartic self-interaction related to the dimer-dimer scattering length, at unitarity we have no scales, and so $g(\rho) \propto \rho^{5/3}$ is required on dimensional grounds, reproducing the UFG EOS. The normalization of the time-evolution equation ensures Galilean covariance.

This modified GPE corresponds to a class of DFTs known as ETF models.[1] In the absence of phase fluctuations, one can show that the model (4) is equivalent to following local Hohenberg-Kohn DFT [33–35]:

$$E[\rho] = \int d3x\left(\frac{\lambda\hbar^2}{8m}\frac{(\nabla\rho)^2}{\rho} + V(x)\rho + \xi\mathcal{E}_{FG}(\rho)\right), \quad (5)$$

which is the more common form for the ETF model. This includes gradient corrections proportional to λ as originally suggested by Weizsäcker [50] which includes both a direct contribution from kinetic energy as well as a correction proportional to $1 - 4\lambda$ that we shall neglect by setting $\lambda = 1/4$ as discussed below.

The ETF model reproduces the quantum hydrodynamics equations [51] which describe the evolution of the density and velocity fields ρ and v:

$$\Psi = \sqrt{\frac{\rho}{2}}e^{2i\phi}, v = \frac{\hbar\nabla\phi}{m} = \frac{\Psi^* i\overleftrightarrow{\nabla}\Psi}{2m\Psi^\dagger\Psi},$$
$$\partial_t\rho + \nabla\cdot(\rho v) = 0, \quad (6a)$$

$$-m\partial_t v = \nabla\left(\frac{mv^2}{2} + V(x) + \xi E_F(\rho) - \lambda\frac{\hbar^2}{2m}\frac{\nabla^2\sqrt{\rho}}{\sqrt{\rho}}\right), \quad (6b)$$

where $\Psi^* i\overleftrightarrow{\nabla}\Psi = (\Psi^* i\nabla\Psi - \nabla\Psi^* i\Psi)/2$. Note that (6b) contains the "quantum pressure": singularities in this term are crucial for describing quantum phenomena such as vortices.

There has been much discussion in the literature [34,35,52,53] about the value of the coefficient of the Weizsäcker term. There are two special values: $\lambda = 1/4$ corresponds to the case where the quantum pressure arises entirely through the kinetic energy, while for $\lambda = 0$ the quantum pressure term in the equation cancels out (6b), reducing the equations to classical hydrodynamics of an

[1]The Thomas-Fermi (TF) approximation to a fermionic DFT corresponds to applying the homogeneous EOS at each point in space, introducing the external potential $V(x)$ as a spatially dependent chemical potential. The "extension" here corresponds to including gradients in the functional. The gradient terms included in (4) represent the lowest-order expansion. See [49] for a discussion.

irrotational and inviscid fluid. For $\lambda = 1/4$ one finds that the condensate near the vortex core goes as $(x + iy)$ [46] (where x, y are the coordinates in the plane perpendicular to the vortex with origin at the core) and better describes the dynamics of colliding superfluids [39]. Hence in this paper we will restrict ourselves to $\lambda = 1/4$. The resulting ETF model is described by a single parameter, the Bertsch parameter ξ. To compare with the time-dependent SLDA simulations of Ref. [14], we will use their value $\xi = 0.42$.

The aim of this paper is to demonstrate the extent to which the ETF can be used to study the dynamics of the UFG in place of the more computationally expensive SLDA. Since the ETF is tuned to match the UFG EOS, it will by construction reproduce all related properties such as the leading-order (LO) (in energy and momentum) static and dynamic responses. The nontrivial validation comes when one considers higher orders and nonlinear effects. We consider three tests here: (Sec. III) the static response at high wave vectors q; (Sec. IV) the dynamic linear response at finite wave vector q and frequency ω; (Sec. V) the nonlinear response by comparing with SLDA dynamics and experiments.

III. STATIC RESPONSE

The static ETF model has been compared with QMC results for the harmonically trapped UFG [34,35]. Comparison with recent QMC results [46] demonstrates that it exhibits the correct qualitative asymptotic behavior in the thermodynamic limit, reproducing the asymptotic form predicted by the low-energy superfluid effective field theory [55], but fails for small systems. This failure is expected since the ETF lacks the fermionic shell structure resulting from the Pauli exclusion principle and the kinetic density τ in the SLDA.

The linearized static density response $\chi_\rho(q,\omega = 0)$ for wave vector q is defined by considering how the density changes in response to a small cosine modulation:

$$V_R(x) = \delta\cos(qx), \quad \rho(x) = \rho_0 + \chi_\rho(q,\omega = 0)\,\delta\cos(qx).$$

The static response of the ETF and SLDA are compared in Fig. 1. The EOS fixes the value $\chi_\rho(q \to 0,\omega = 0) = \partial n/\partial\mu$, but the ETF matches the fermionic SLDA quite well, even for large wave vectors. Although we do not consider such corrections here, it should be possible to add gradient corrections to the ETF to improve this agreement (being careful not to affect the structure of vortices near the core, etc.).

To compare the static response in the nonlinear regime, we consider the structure of a single vortex in Fig. 2. This demonstrates one major limitation of the ETF model which imposes an artificial relationship between the square of the order parameter and the density $\rho = 2|\Psi|^2$. In the fermionic theory, the relationship between Δ and ρ are determined as independent sums of the single-particle wave functions: the relation $\rho = 2|\Psi|^2$ only becomes valid for fermions in the deep BEC regime. In the UFG, the vortex cores have a nonzero density (often thought of as "normal" fermionic modes occupying the vortex core where the superfluid condensate vanishes), while the ETF by construction has zero-density wherever the condensate $\Psi = 0$ vanishes.

This core occupation also appears in solitons, giving rise to a change in the oscillation period for solitons in a quasi-1D harmonic trap from $T \approx \sqrt{2}T_z$ [57–61] in the bosonic systems (reproduced by the ETF model) to $T \approx \sqrt{3}T_z$ in the fermionic DFTs (BdG [62] and SLDA [63]). Thus, bosonic and fermionic simulations are qualitatively, but not quantitatively, similar when describing these types of dynamics. Note that a recent experiment [10] suggested that solitons in the UFG might have a significantly longer period $T \approx 10T_z$, but this has been resolved by identifying the observations with vortex rings [15].

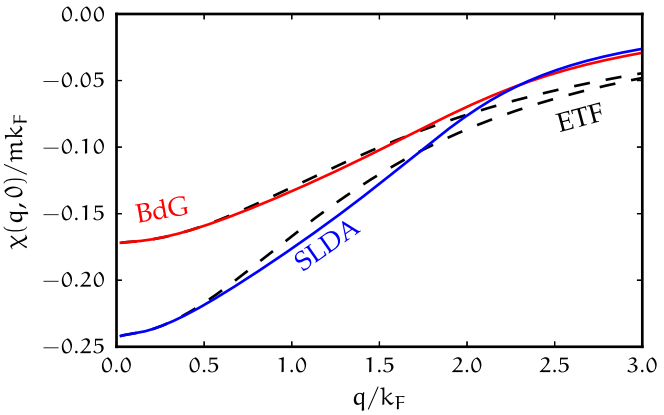

FIG. 1. (Color online) Static ($\omega = 0$) response for two fermionic DFTs and the corresponding ETFs. Upper curve: BdG (upper solid red curve) with $\xi = 0.5906\cdots$ and $\Delta = 0.6864\cdots E_F$ (see also [54]). Lower curve: SLDA (lower solid blue curve) with $\alpha = 1$, $\xi = 0.42$, and $\Delta = 0.502E_F$ (to match [14]). The ETFs (dashed black curves) have their single parameter ξ tuned to match the respective fermionic theories, and consequently match at $q = 0$ where the response (the compressibility) is determined by the EOS. The curvature for small q is incidentally numerically very similar for the corresponding theories (see Sec. IV). The deviations for larger q give an estimate of how well the ETFs can model the fermionic theories.

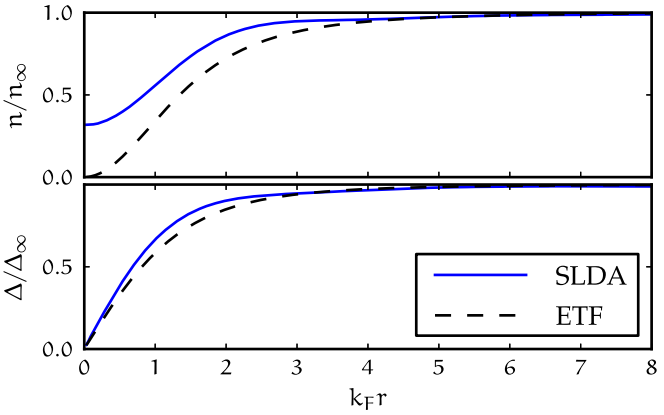

FIG. 2. (Color online) Structure of a single static vortex in the SLDA [56] (solid blue curve), and in the matching ETF (dashed black curve). We compare only with parameter set II from [56] which has unit inverse effective mass $\alpha = m/m_* = 1$ and parameters tuned so that $\xi = 0.44$ while the energy of the normal state is $\xi_N = 0.54$ (this gives a somewhat low pairing gap $\Delta \approx 0.3718E_F$). We do not consider the $\alpha \neq 1$ vortex for parameter set I in [56] which is missing the corrections that restore Galilean invariance [30].

Related to the deficiency in properly describing the core density, we note that unitary evolution of the ETF implies that

$$\frac{\partial}{\partial t}\int d^3\boldsymbol{x}\,\Psi^*(\boldsymbol{x},t)\Psi(\boldsymbol{x},t)=0. \tag{7}$$

This means that not only is the total particle number conserved (which is physical), but the integrated "gap" is also conserved. In fermionic systems, pair-breaking excitations will reduce the gap, resulting in a mixture of superfluid and normal fluid; in highly excited systems the superfluid may vanish completely. The ETF on the other hand does not admit this behavior, and even highly excited systems will still have a rapidly fluctuating but nonzero order parameter. The degree to which the integrated gap is conserved during the evolution of a fermionic system provides a useful measure of how successfully the ETF can model the corresponding evolution. (We shall explore this further in Fig. 8.)

Despite the fact that the resulting ETF contains only a single parameter (compared with the three independent parameters of the SLDA), it still qualitatively reproduces many response properties. This qualitative agreement is a somewhat fortuitous consequence of the best-fit parameter values. From the point of view of the ETF, the UFG contains two independent length scales: the interparticle spacing set by the density, and the coherence length set by the gap. This is demonstrated by the failure of the ETF to capture the core structure of a vortex. Thus, while the present concordance of the SLDA and ETF is fortuitous, it may turn out that the SLDA requires further gradient corrections [46] (a result that is still awaiting further *ab initio* confirmation). If these corrections turn out to be significant, then one might have to introduce gradient corrections in the ETF in a more complicated form (compared to the simple Weizsäcker term) that does not spoil vortex structure and collision dynamics. Such corrections will be nonuniversal (i.e., must have a different form for small densities than for large densities) and probably most conveniently accounted for in a two-fluid model with an additional "normal" component that can populate the vortex core. The approximation to the BdG discussed in [64] may shed some light on the nature of these types of corrections.

IV. LINEAR RESPONSE

We now consider dynamical systems. For small fluctuations one can simply compare the linear response of the ETF with that of the SLDA. We compute the response of the system to an external time-dependent perturbation in the limit of small δ:

$$V_R(x,t)=\delta\mathrm{Re}[e^{i(qx+\omega t)}],$$
$$\rho_R(x,t)=\rho_0+\delta\mathrm{Re}[\chi_n e^{i(qx+\omega t)}]+O(\delta^2).$$

The magnitude of the resulting response $|\chi_n|$ is shown in Fig. 3 for the BdG and SLDA and compared with the response for the corresponding ETF model tuned to match the value of ξ.

The response at low frequencies is dominated by the pole associated with the superfluid phonon. This may be computed analytically for homogeneous matter in the ETF:

$$\omega_{\mathrm{phonon}}=\sqrt{\left(\frac{\hbar q^2}{4m}\right)^2+\frac{2q^2}{3m}\xi E_F}=c_s q+O(q^3), \tag{8}$$

where $c_s=\sqrt{\xi/3}v_F$ is the sound speed and $v_F=\hbar k_F/m$ is the Fermi velocity. At small momenta, q, the f-sum rule [65] ensures that the residue of the pole in the bosonic and fermionic theories is equal to $-\pi\rho_0 q^2\hbar^2/(2m\omega)$.

The low-energy properties of these theories can be characterized by a superfluid effective field theory for the UFG [55] (also see [66]). At LO, the theory is characterized by the Bertsch parameter ξ which determines the equation of state. Two new coefficients appear at next to leading order (NLO),[2] which we shall denote c_χ and c_ω following [46], that characterize the low-energy static and dynamic properties, respectively. These coefficients characterize the phonon dispersion ω_q and static response $\chi(q,\omega=0)$:

$$\omega_q=c_s q\left[1+\frac{c_\omega}{24\xi}\frac{q^2}{k_F^2}+O(q^4\ln q)\right], \tag{9}$$

$$\chi(q,\omega=0)=\frac{-mk_F}{\hbar^2\pi^2\xi}\left[1-\frac{c_\chi}{12\xi}\frac{q^2}{k_F^2}+O(q^4\ln q)\right]. \tag{10}$$

Matching with the linear response of the ETF gives $c_\omega=c_\chi=9/4$. This is qualitatively consistent with the estimate of these parameters from the ϵ expansion [67] (expanding in spatial dimension: $\epsilon=4-d$) which finds $c_\chi\approx 8/5+O(\epsilon^2)$ and $c_\chi\approx c_\omega+O(\epsilon^2)$.[3] The BdG mean-field theory [66] finds quite different values, $c_\chi=7/3$ and $c_\omega=0.7539$. Interestingly, for $\alpha=1$ the SLDA gives $c_\chi=7/3$ independent of the values of β and γ in Eq. (2) (or equivalently η and ξ). The value of c_ω in SLDA is not quite as robust. For fixed $\eta=0.502$ and $\alpha=1$, c_ω changes from -0.255 to 0.055 as ξ is reduced from 0.42 to 0.37 (i.e., from the value used in Fig. 3 to the current best-fit value). The value for $c_\chi\approx 1.5(3)$ follows from an analysis of gradient corrections to harmonically trapped gases [46].

The value of c_ω determines the curvature of the phonon dispersion. As is clear from Fig. 3 the ETF gives a large positive curvature for the dispersion. In contrast the dispersion curves for BdG and SLDA appear relatively linear and eventually curve downward. This is a combination of two effects. First, c_ω is smaller in the fermionic theories (negative for SLDA). Second, higher-order effects in q/k_F pull the curves down as one approaches the pair-breaking threshold. For the BdG this implies the existence of a point of inflection at $q/k_F\approx 0.53$.

That the ETF has no transverse response, which can be expressed in terms of the difference $c_\chi-c_\omega$, represents another shortcoming of the model. As argued in [55], the transverse response should be positive to ensure stability with respect to a spontaneous generation of currents or formation of inhomogeneous condensates.

[2]The coefficients c_χ and c_ω are "natural" in the sense that $c_\chi\approx c_\omega\approx 1$. Different notations are used in [55] and [66]; both use $\xi=2^{5/3}/(15c_0\pi^2)^{2/3}$: $\frac{c_\chi}{-6\pi^2(2\xi)^{3/2}}$ is $2c_1-9c_2$ in Ref. [55], but $2c_1$ in Ref. [66] $\frac{c_\omega}{-6\pi^2(2\xi)^{3/2}}$ is $2c_1+3c_2$ in Ref. [55], but $2c_1-6c_2$ in Ref. [66].

[3]To compare with [67], note that their $c_s\equiv c_\chi/2\xi$.

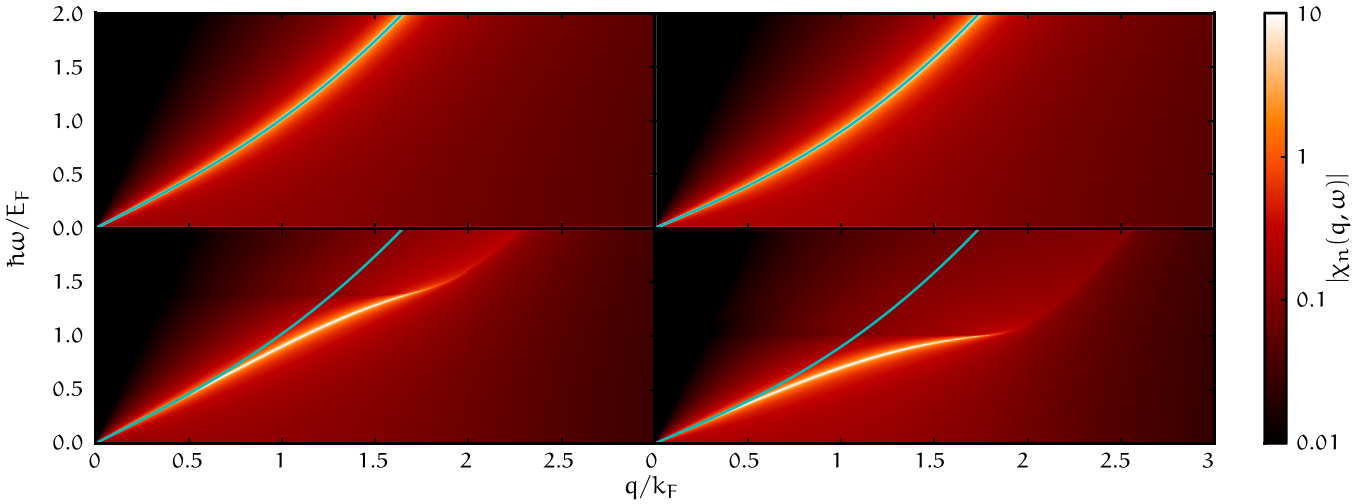

FIG. 3. (Color online) Comparison of the linear response for the ETF (top) and two fermionic DFTs (bottom). The linear response of the BdG which has $\xi = 0.5906\cdots$ and $\Delta = 0.6864\cdots E_F$ (see also [54]) is on the lower left; the linear response of the SLDA tuned to $\xi = 0.42$ and $\Delta = 0.502E_F$ to match [14] is on the lower right. The ETF has only the single tunable parameter ξ, which is chosen to match the corresponding fermionic theory in the panel immediately below. The bosonic ETF reproduces the low-frequency response, but breaks down for $\omega \approx 2\Delta$ at the pair-breaking threshold. The slope of the phonon dispersion relationship is reproduced near the origin, but the curvature differs between the fermionic and bosonic theories.

To end this section, we consider the numerical values using $\xi = 0.374$ [25]:

$$\omega_q \propto 1 + 0.11c_\omega \frac{q^2}{k_F^2}, \quad \chi(q) \propto 1 - 0.22c_\chi \frac{q^2}{k_F^2}.$$

Since $c_\chi \approx c_\omega \sim 1$, we see that the prefactor multiplying the correction to the leading-order dynamics is somewhat small. Thus the low-energy dynamics are rather insensitive to the limitation that $c_\chi - c_\omega$ vanishes in the ETF and that c_ω is somewhat larger than in fermionic theories. The partly explains the success that the ETF enjoys at low energy.

V. NONLINEAR RESPONSE

From the previous analysis, we expect the ETF to provide a reasonable description of small-amplitude fermionic dynamics as long as one does not push the system to the pair-breaking threshold, i.e., for slowly varying external potentials. In the nonlinear regime, the disagreement grows as evolution in the ETF transfers energy from the small-momentum modes to the higher-momentum modes. The high-momentum response is dominated by the phonon dispersion, so this tends to create excitations in the pair-breaking regime where the ETF breaks down.

The transfer of energy to higher momenta results from the nonlinear interaction term which acts as a wave-vector multiplier. The result is that ETF simulations tend to be more noisy than the corresponding SLDA simulations. To see this in a concrete example, we directly compare the dynamics of the ETF with that of the SLDA using the same trapping potential and time-dependent stirring potential as in [14].

The setup is as follows: The cloud is prepared in the ground state of a two-dimensional axially symmetric flat-bottomed trap of radius R (precise details of the potential, etc., are given in Appendix B). A repulsive potential at a distance r_{stir} from the center rotates with constant angular frequency $\omega_{\text{stir}} = v_{\text{stir}}/r_{\text{stir}}$. This is gradually turned on, left on for $n_{\text{stir}} \approx 10$ rotations, then gradually turned off. These simulations are quasi-two-dimensional and have translational symmetry along the trap axis: the fermionic simulation discretizes the wave functions on a 32^2 two-dimensional lattice. It will turn out that simulating the ETF on larger (64^2) lattices better reproduces features of the fermionic theory, most likely due to the transfer of energy to higher-momentum modes discussed above. Figure 4 summarizes some sample results.

In Table I we compare the number of vortices generated after four (for $v_{\text{stir}} = 0.1, 0.11$) or ten revolutions (for all others) of the stirring potential. The table demonstrates the

TABLE I. Number of vortices created after ten revolutions of a stirring potential as a function of the stirring velocity v_{stir}/v_F where v_F is the Fermi velocity at the center of the trap. The second column (SLDA) shows the results of [14] on a 32^2 lattice, while the third and fourth columns show the corresponding results for the ETF with lattices of 32^2 and 64^2 points, respectively. For the higher velocities, the 32^2 ETF simulations are too noisy to admit an accurate count of the vortices.

v_{stir}/v_F	SLDA (32^2)	ETF (64^2)	ETF (32^2)
0.1	1	0	0
0.11		1	1
0.197		3	2
0.2	3	4	3
0.242		5	2
0.25	5	6	2
0.3	6	5	(noise)
0.312		6	(noise)
0.35	7	7	(noise)
0.40	9	9	(noise)

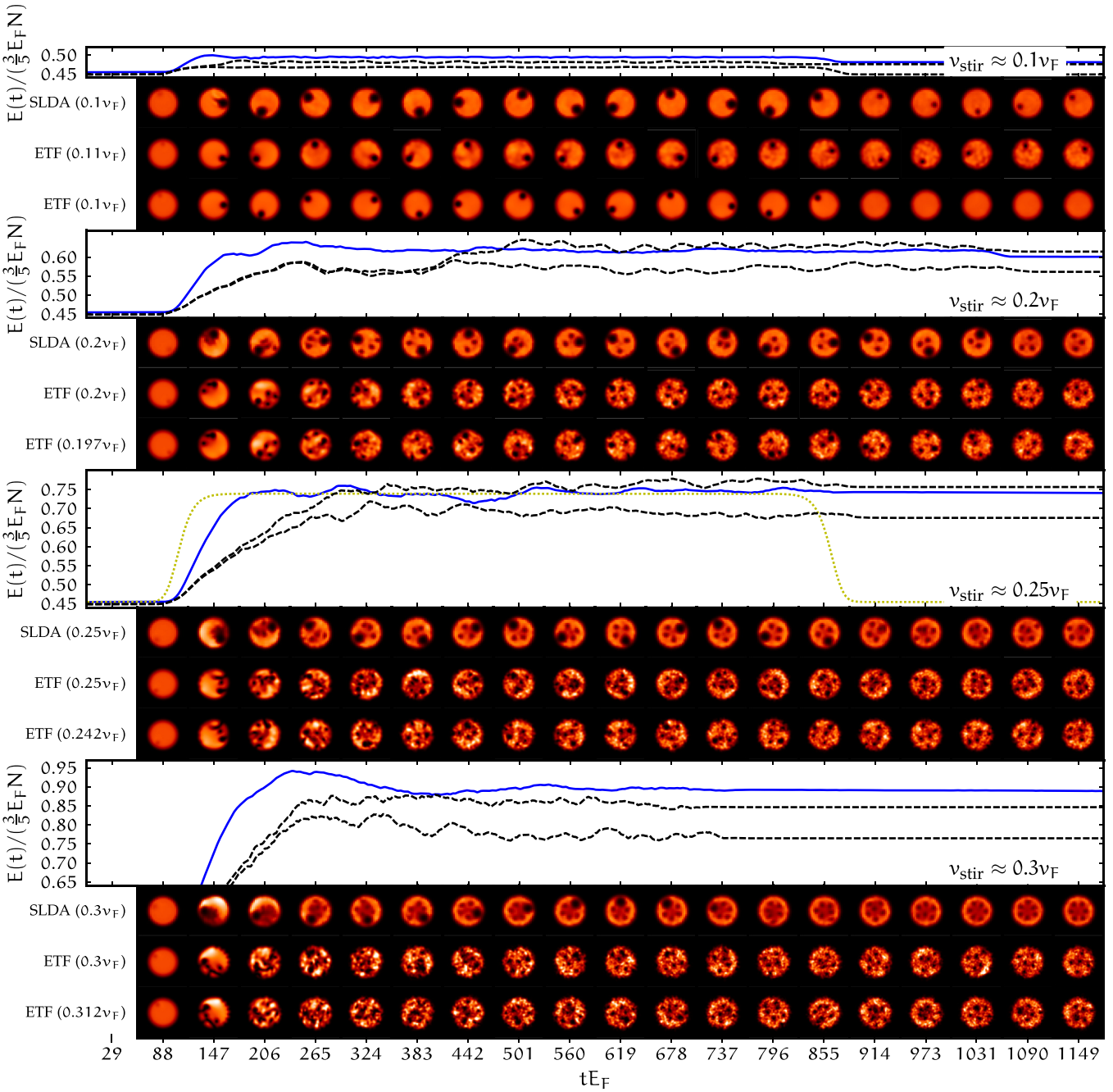

FIG. 4. (Color online) Stirring simulations. The curves show the energy per particle as a function of time for various simulations for increasing stirring speeds: $v_{\rm stir} \approx 0.1 v_F$ (top), $v_{\rm stir} \approx 0.2 v_F$, $v_{\rm stir} \approx 0.25 v_F$ (middle), and $v_{\rm stir} \approx 0.3 v_F$ (bottom). Sample density profiles are shown below the x axis starting with the SLDA simulation from [14], followed by the ETF simulation(s). The plots each have two ETF simulations, one with exactly the same $v_{\rm stir}$ as the SLDA, and another with a slightly different $v_{\rm stir}$ that produces the same total number of vortices and give the energy curves (dashed, black) immediately below the SLDA energy curves (solid, blue). The SLDA simulations use a 32^2 lattice while the ETF simulations use a 64^2 lattice. The light dotted (yellow) curve in the third plot shows the strength of the stirring potential (in arbitrary units) as it is turned on, held, then turned off.

qualitative agreement between the ETF model and the SLDA. For small velocities, there are some minor disagreements: at $v_{\rm stir} = 0.1$, the ETF does not produce a vortex, but does produce one for $v_{\rm stir} = 0.11$. This $\approx$10% difference might be due to differences in the static response of the ETF and the SLDA. For example, the pinning potential creates a larger depletion in the SLDA (visible in Fig. 4), thereby exciting regions closer to the edge of the trap where the density is lower. These regions have a slower critical velocity, allowing a vortex to be nucleated more easily than in the ETF. One might consider tuning the potential or model as suggested in [32] to study vortex-pinning interactions to match the density depletion in the ETF to that in the SLDA, but we have not performed any such tuning here.

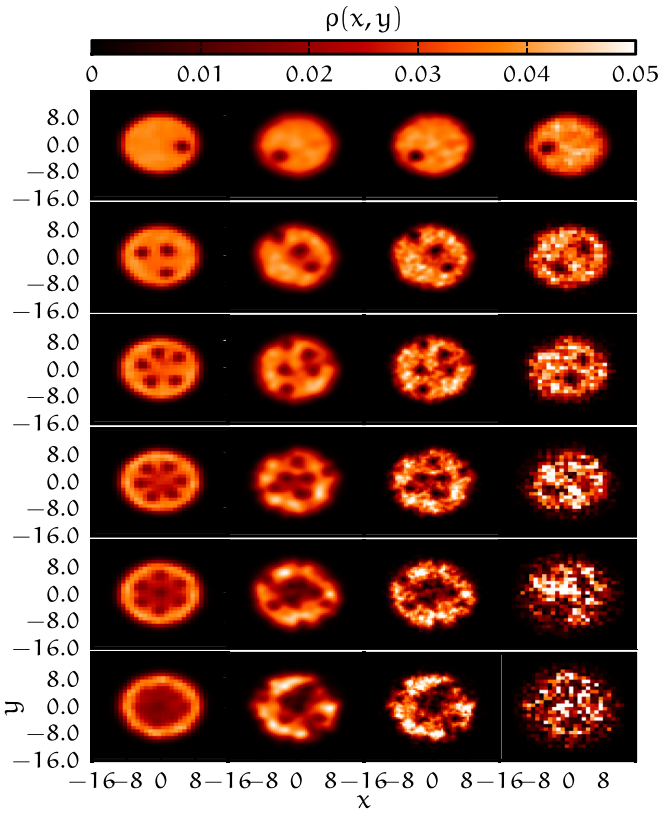

FIG. 5. (Color online) Comparison of final-state densities (moving from left to right) for $N = 32$ SLDA, a smoothed version of $N = 64$ ETF, the raw result for $N = 64$ ETF, and the raw result for the $N = 32$ ETF. The simulations are for $v_{\text{stir}} \approx 0.1, 0.2, 0.3, 0.35, 0.40$ (moving from top to bottom), taking the v_{stir} for the ETF from Table I which gives the same number of vortices as the SLDA. The SLDA vortices are arranged in a regular pattern in the final state. The $N = 32$ ETF is too noisy. The higher resolution ($N = 64$) ETFs are qualitatively more similar, especially after smoothing, but the vortices are not as regularly arranged as the SLDA simulations. The density was smoothed by convolving with a two-dimensional Gaussian smearing function of spatial width $0.75/k_F$. The length of each side of the system is 32 units for both $N = 32$ and $N = 64$.

As one increases the rotation rate, one finds that the 32^2 simulations depart significantly; these essentially develop short-wavelength noise due to the aforementioned amplification of short-wavelength modes to a point where identifying vortices becomes impossible. The problem here is essentially that significant phonon "noise" coexists on the same length scale as the vortex core. Increasing the resolution resolves this issue by providing a separation of scales between the phonon "noise" and the larger structure of the vortices. A comparison of the final states obtained for various resolutions is shown in Fig. 5.

The rough final agreement in vortex number between the two theories follows mainly from the superfluidity of the system. In order to support a rotational current with a fixed stirring velocity v_{stir} at the specified radius, the system must carry enough angular momentum; hence it must have (roughly) a certain number of vortices. Once the system achieves a rotational flow with $v = v_{\text{stir}}$ an equilibrium is established and no further energy is transferred from the stirrer to the system. From Fig. 4 we see that the overall energy scale for a given number of vortices is roughly equal in the ETF and the SLDA (the final ETF energies are systematically slightly smaller than the final SLDA energies for the same number of vortices). This is because the equation of state of the two systems are the same and energies are the kind of bulk property for which the ETF can be trusted.

From the details in Fig. 4, this bulk agreement is apparent. In addition, one sees detailed qualitative agreement in the dynamics for lightly excited systems. For example, the single vortex produced for $v_{\text{stir}} \approx 0.1 v_F$ behaves almost identically in both the SLDA and ETF. While the stirrer is "on," the vortex is closely attached to it. When the stirrer has "switched off," the vortex continues (roughly) rotating around the center of the trap with an angular velocity $\omega \sim \hbar/[2m(R^2 - r_{\text{stir}}^2)]$ determined by the background superfluid velocity at the vortex induced by the trap [17].

For higher velocities, however, many qualitative differences between the SLDA and ETF dynamics become apparent. Most obviously, the energy transfer to the ETF is significantly slower in the ETF than in the SLDA. Another obvious feature is that the ETF vortex lattice does not "crystallize" as it does in the SLDA. This is similar behavior to the GPE where crystallization is known to require the addition of dissipative mechanisms as in the stochastic Gross-Pitaevskii equation (SGPE) (see [68] and references therein).

The nonlinear nature of the ETF implies that even if initially only long-wavelength modes are excited (for example, in our simulations the stirring potential only only has support for momenta up to $q/k_F \lesssim 1.5$), energy can be transferred to short-wavelength modes. This phenomenon is common to a variety of nonlinear nondissipative systems, for instance optical systems, cold plasmas, and bosonic superfluids described by the GPE [69]. The difficulty this presents with the ETF is that the phonon pole continues to extend to both high momenta and high frequencies, whereas in the SLDA, the pole is replaced by a branch cut at the pair-breaking threshold (see Fig. 3). Thus, while short-wavelength modes seem to decay in the SLDA, they persist (see Fig. 6) in the ETF giving rise to

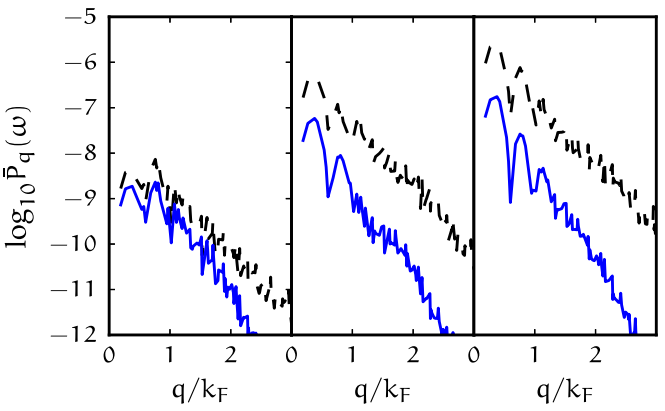

FIG. 6. (Color online) Comparison of the power spectrum (averaged over the time after "switch off") for different momentum modes for the SLDA and the ETF. The fluctuations in the SLDA decrease with increasing q faster than in the GPE.

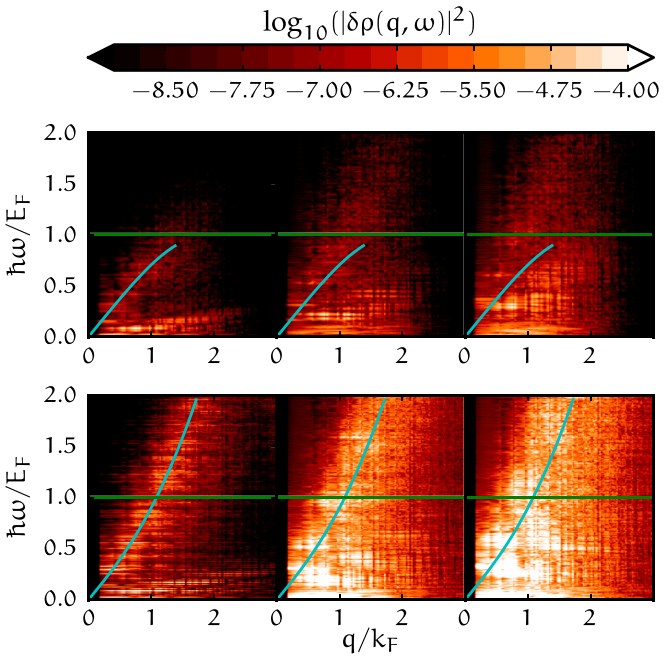

FIG. 7. (Color online) We compare the power spectra of the fluctuations of density in the bosonic simulations (lower panel) and the fermionic simulations (upper panel). For the bosonic (fermionic) simulations we consider stirring velocities $v_{\rm stir} = 0.11v_F$ $(0.10v_F)$, $v_{\rm stir} = 0.197v_F$ $(0.20v_F)$, and $v_{\rm stir} = 0.242v_F$ $(0.25v_F)$, going from left to right. The spatial Fourier transform is taken over the entire simulation volume and the temporal transform is taken over the time after the stirring potential is turned off. The solid horizontal line (green) corresponds to the pair-breaking threshold, $\omega/E_F = 2\eta$. For the SLDA simulations, there is little strength above the pair-breaking threshold. For the ETF simulations with the smallest velocity, most of the power is concentrated in the low frequencies. For higher velocities, there is significant power near and above the pair-breaking threshold. The curves (blue) correspond to the phonon dispersion relation.

noisy simulations that cannot reproduce features such as the relaxation of vortex lattices (see Fig. 5).

To contrast the situation from the SLDA we compare the power spectra of the density perturbations in Fig. 7. These spectra are computed after the stirring potential is turned off and demonstrate that the majority of the power lies along the phonon dispersion. These simulations also have vortices, which add power at low frequencies (one can think of a vortex as a collection of virtual phonons). Note that in the ETF, even the slowest simulation $v_{\rm stir} = 0.11v_F$ has energy above the pair-breaking excitation, demonstrating the amplification of short-wavelength modes.

All of this evidence is commensurate with the fundamental failure of the ETF to properly describe pair-breaking excitations above $\omega > 2\Delta$ that appear to be present in all simulations (except the vortexless $v_{\rm stir} = 0.1$ simulation). In the SLDA, these excitations break superfluid pairs, transferring energy to the normal component of the fluid which is absent in the ETF. This provides a damping mechanism for the superfluid in the SLDA that allows the vortex lattice to crystallize. In the ETF, these excitations must remain in the superfluid and scatter off of the vortices, preventing the lattice from crystallizing.

To check this, we can consider the superfluid order parameter Δ. To make its dimensions match with the ETF order parameter we compare the conservation of the following integrated quantities:

$$\text{SLDA: } \int d^3\boldsymbol{x}\ \frac{|2m\Delta|^2}{\rho^{1/3}}, \quad \text{vs} \quad \text{ETF: } \int d^3\boldsymbol{x}\ |\Psi|^2. \quad (11)$$

The scaling has been chosen so that in the Thomas-Fermi limit both the integrals are proportional to the total number of particles. Pair-breaking effects reduce the amount of superfluid, resulting in a decrease in the total integrated gap in the SLDA, whereas the corresponding quantity in the ETF is proportional to the conserved particle number (7).

To realize pair-breaking physics in an ETF-like model, one needs to introduce an additional thermal "normal" component to the system, transferring energy and mass to this as excitations exceed the pair-breaking threshold. To test the validity of this notion, we compare in Fig. 8 the evolution of the integrated pairing gap (11) in the SLDA with the integrated order parameter in the ETF after coarse-graining the field Ψ with a filter that removes excitations above $q \gtrsim 1.3k_F$. (We simply smoothed the 64^2 simulation with a two-dimensional Gaussian smearing function of spatial width $0.75/k_F$.)

The qualitative agreement here shows that this characterization of the superfluid to normal conversion is reasonable. This is visually confirmed in Fig. 5 where we also include a coarse-grained representation of the density (smoothing now the density $\rho = 2|\Psi|^2$ rather than Ψ).

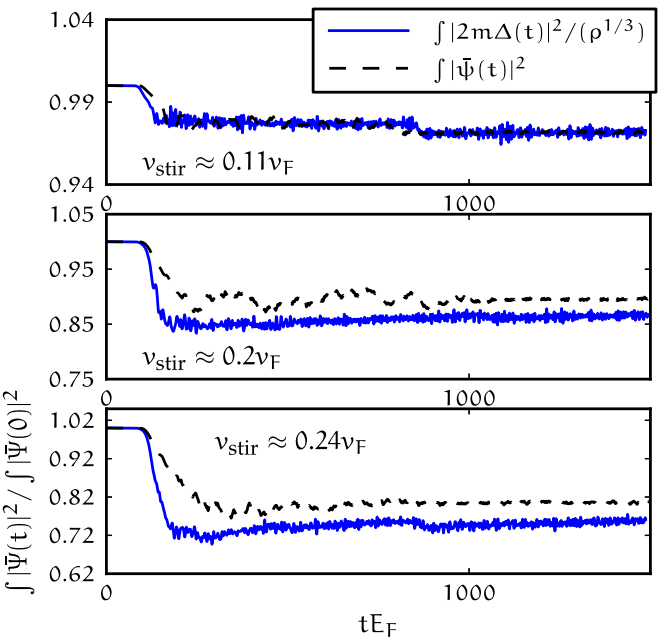

FIG. 8. (Color online) Conservation of the integrated squared pairing gap (squared smoothed ψ) for the simulations for $v_{\rm stir} = 0.1v_F$ $(v_{\rm stir} = 0.11v_F)$, $v_{\rm stir} = 0.2v_F$ $(v_{\rm stir} = 0.197v_F)$, and $v_{\rm stir} = 0.25v_F$ $(v_{\rm stir} = 0.242v_F)$ for SLDA (ETF). The wave function was smoothed by convolving with a two-dimensional Gaussian smearing function of spatial width $0.75/k_F$. Note that the scales of the three plots are different: The $v_{\rm stir} \sim 0.1v_F$ integral is essentially unchanged, while the $v_{\rm stir} \sim 0.25v_F$ integral decreases by about 25%.

A similar coarse graining of the evolved ETF was performed in [39] to compare with the shock-wave experiment [9]. The agreement there confirms this picture that the ETF is suitable for modeling bulk dynamical properties. Note, however, that the difference in dynamics here is in contrast with the implied claim of Refs. [39] that the coarse graining is simply needed to replicate the averaging implied by imaging. Contrasting the vortex dynamics here suggests that the actual motion of topological defects through the Fermi gas cannot be properly modeled by the simple ETF. The agreement seen between [39] and [9] thus supports the conclusion that these differences do not affect bulk dynamical properties.

Coarse graining also adds density to the core of vortices, bringing the density more closely in line with that of the SLDA. In a proper two-fluid model, these effects would increase the effective mass of topological defects, for example, altering their dynamical behavior as was observed for soliton dynamics.

The degree to which the integrated gap $\int |\Delta|^2/\rho^{1/3}$ is conserved provides a measure of the extent to which one can trust the qualitative results of the ETF model, and Fig. 8 shows that a reasonable estimate of this can be obtained from $\int |\bar{\Psi}|^2$ where $\bar{\Psi}$ is Ψ smoothed on a scale of $q \approx 1.5k_F$; i.e., $\bar{\Psi}$ is the result of applying a low-pass filter to Ψ excluding Fourier components with $k > 1.5k_F$. Of course, one can also extract this information from the spectra (Fig. 7) but the nonconservation of the integrated gap provides a convenient representation.

To see that this diagnostic applies in other geometries, we consider the success of [39] where the ETF quantitatively describes the evolution of the densities observed in the experiment [9] which collides two clouds of the unitary Fermi gas. Checking the diagnostic on one-dimensional and two-dimensional realizations of this experiment, we find that $\int |\bar{\Psi}|^2$ is conserved on the subpercent level, providing evidence that this criterion is applicable for generic traps, especially where the potential does not have large gradients.

VI. CONCLUSION

We study the features and the limitations of the ETF as a model for the dynamics of unitary Fermi gases by comparing and contrasting its dynamical properties with those of the fermionic SLDA DFT from [14]. Like the GPE, the dynamical ETF model depends on a single collective wave function Ψ; it is therefore significantly easier to solve numerically than the SLDA which requires evolving hundreds of thousands of wave functions. Unlike the SLDA, however, the ETF lacks a pair-breaking mechanism. The extra fermionic degrees of freedom in the SLDA allow it to model both the superfluid and the normal components whereas the ETF models only the superfluid.

By comparing the dynamic response of the ETF with that of the SLDA, we can assess the importance of these pair-breaking effects on the overall dynamics. We find that the ETF and SLDA have similar properties at low energies with a similar static response (Fig. 1) on the 10% level even for momenta q about $2k_F$. The dynamic linear response (Fig. 3) is also similar for small momenta and frequencies as required by the equation of state, but significantly departs near the pair-breaking threshold $\omega \sim 2\Delta$. We also remark on a possible physical consequence of the difference in the curvatures of the phonon dispersion curves, as elucidated by Fig. 3. In a theory with positive curvature, the phonon with higher energy is kinematically allowed to decay to multiple phonons of lower energy. We can see that the curvature of the dispersion relation in ETF is positive. On the other hand, for $\xi = 0.42$, $\eta = 0.502$, and $\alpha = 1$ the phonon dispersion in the SLDA has a negative curvature. To see physical implications of these differences, however, one must devise sensitive probes as the effect is naturally quite small. We note that such decays will not show up in a theory like the ETF where the fluctuations about the condensate—the phonons—are not quantized, but will be present if we describe phonon dynamics using any transport formalism.

Exciting the ETF produces phonons and topological defects (vortices in this case), but nonlinear excitations amplify the amplitudes of the high-frequency modes, thereby creating excitations above the pair-breaking threshold. Once a system contains appreciable power above the pair-breaking threshold, detailed dynamics of topological defects disagree markedly between the two theories; vortex lattices crystallize in the SLDA, for example, but remain chaotic in the ETF.

Despite these differences in microscopic behavior, the ETF remains a useful tool for modeling bulk dynamics. This is perhaps best demonstrated by the remarkable quantitative agreement between the ETF simulations [39] and the observed shock-wave phenomena obtained experimentally by colliding two UFG clouds [9]. The quantitative agreement conclusively demonstrates that [9] is not probing dissipative effects such as viscosity which are missing in the conservative ETF approach.

The picture that emerges is that the high-frequency, short-wavelength phonon gas in the ETF acts very much like the excited "normal" component created through pair breaking in the SLDA. This suggests that one might be able to improve a simple model like the ETF by somehow introducing a normal component and a coarse-graining process that transfers energy and particle number from the superfluid to this normal component, such as realized for bosonic systems with the SGPE and the stochastic projected Gross-Pitaevskii equation (SPGPE) (see Refs. [68] and references therein). This is further confirmed by coarse graining the ETF results which results in a much better qualitative agreement with the SLDA. One effect of coarse graining is to add density in the cores of topological defects; thus, a theory that effectively coarse grains should better reproduce the dynamics of fermionic defects which have a different effective mass. Another effect is the reduction in the integrated square of the coarse-grained order parameter, mimicking the conversion of the superfluid to a normal fluid. The qualitative agreement of this reduction also provides a diagnostic for assessing how well a given ETF simulation might model dynamics in the SLDA.

We have considered only zero-temperature dynamics here; it is an interesting question as to how finite-temperature dynamics might be implemented in a similar framework, and to what extent coarse graining can describe thermalization. SGPE and SPGPE (Refs. [68,70]) provide a natural starting point for such an investigation. The extension of SLDA to finite temperatures—evolving thermally occupied ensembles—is another possible direction.

ACKNOWLEDGMENTS

We thank A. Bulgac and A. Luo for useful discussions and sharing their data. This work is supported, in part, by US Department of Energy (DOE) Grant No. DE-FG02-00ER41132 and by the Natural Sciences and Engineering Research Council of Canada (NSERC).

APPENDIX A: NUMERICAL IMPLEMENTATION

Almost any algorithm implementing the GPE can be easily extended to implement the ETF; the only differences are the form of the nonlinear interaction ($\rho^{5/3}$ vs ρ^2) and a few factors of 2. We implement the evolution using two methods: if high-accuracy is needed (in order to calculate a power spectrum for example), then we use a fifth-order integrator described in [71] that averages the Adams-Bashforth and Milne (ABM) predictor-corrector methods:

$$\begin{aligned} p_{n+1} &= \frac{y_n + y_{n-1}}{2} + \frac{h}{48}(119y'_n - 99y'_{n-1} \\ &\quad + 69y'_{n-2} - 17y'_{n-3}) + \frac{161}{480}h^5 y^{(5)}, \\ m_{n+1} &= p_{n+1} - \frac{161}{170}(p_n - c_n), \\ c_{n+1} &= \frac{y_n + y_{n-1}}{2} + \frac{h}{48}(17m'_{n+1} + 51y'_n \\ &\quad + 3y'_{n-1} + y'_{n-2}) - \frac{9}{480}h^5 y^{(5)}, \\ y_{n+1} &= c_{n+1} + \frac{9}{170}(p_{n+1} - c_{n+1}), \end{aligned} \tag{A1}$$

where $h = \delta_t$ is the time step. Here the primes denote derivatives as computed with the Hamiltonian: $y'_n = \partial_t y_n = -i\boldsymbol{H} y_n$. Each iteration requires two applications of the Hamiltonian, one for the predicted step m'_{n+1} (evaluated at time $t + h/2$) and one for the corrected step y'_{n+1} (evaluated at time $t + h$). Note that y_{n+1} is accurate to order h^6, so after iterating by $N = T/h$ steps, one obtains an error that scales as h^5 (fifth order). This scaling requires that the function be at least $\mathcal{C}^{(4)}$, so a high-order integrator must be used to provide the first four stating iterations. (Another approach is to start from a stationary solution so that $y_m = p_m = c_m = y_0$ for $n \in \{1,2,3\}$).

This method requires storing the previous four derivatives y'_{n-3}, y'_{n-2}, y'_{n-1}, y'_n, as well as the previous $p_n - c_n$ and current and previous steps y_n, and y_{n+1}. Adding an additional workspace for computing the fast Fourier transform (FFT), the memory requirements rise to $8N$ complex numbers.

When one does not need high accuracy, an alternative method, the split-operator approach, is faster. Here one decomposes the Hamiltonian into kinetic and potential parts, each of which can be applied directly to the wave function with an error that scales as h^3 [72]:

$$e^{i\hbar h(\boldsymbol{K}+\boldsymbol{V})} = e^{i\hbar h\boldsymbol{K}/2} e^{i\hbar h\boldsymbol{V}} e^{i\hbar h\boldsymbol{K}/2} + O(h^3). \tag{A2}$$

This method is symplectic, effecting strictly unitary evolution, and requires no additional storage beyond the current state and any scratch space needed for computing the FFT. In addition, this approach can be nicely transferred to a graphics processing unit (GPU) for a further gain in performance. Although not as accurate as the higher-order ABM method, this method can be used with relatively large time steps ($h = \delta_t \approx 0.1/\hbar E_c$) to quickly gain a qualitative picture of the dynamics.

APPENDIX B: PARAMETERS OF THE TRAP

To compare our results with Ref. [14] we use $\xi = 0.42$ in Eq. (4). The parameters are conveniently written in "atomic" units, where we take $\hbar = m = 1$. The chemical potential is chosen so that the ground-state density of fermions, ρ, at the center of the trap matches the desired value, $\rho_{\text{central}} = 0.0375$, which corresponds to $k_F = 1.035$ ($E_F = 0.536$). This fixes the chemical potential $\mu = \xi E_F = 0.225$.

The trapping potential is cylindrically symmetric and taken to have the same profile as used in [14],

$$V(r) = 3.9478 \times \left[\frac{1 - \cos\frac{2\pi r}{L}}{2}\right]^8, \tag{B1}$$

where $L = 32$ is the extent of the simulation box in each direction, and r is the distance from the center.

The trap radius R is defined as the point where $V(r/0.90) = \mu$, where the factor of 0.9 is used to avoid the periphery of the cloud. This gives $R = 9.08$. We focus on the family of simulations performed in [14] for $N = 32$ grid points in each (x and y) direction. To compare, we perform simulations for $N = 32$ and $N = 64$ points in each direction. In Table I, the trap has radius $R = 9.08$ and the stirrer orbits at fixed distance $r_{\text{stir}} = 6$ from the center.

We begin the simulation with the ground state in the potential (B1) at time $t = 0$. If the Thomas-Fermi profile were exact in both SLDA and the GPE, the density profiles of the two would be equal. In reality, the density profiles differ near the boundary of the trap and the total number of particles in the GPE ($N_{\text{part}} = 9.047$ per unit length, or 289.5 particles in a cylinder of height 32) differs slightly from the total number in the SLDA ($N_{\text{part}} = 9.375$ per unit length, or 300 particles in a cylinder of height 32).

A stirring potential of the form

$$V_{\text{stir}} = E_F \exp\left(-\frac{r^2}{r_{\text{pin}}^2}\right) \tag{B2}$$

with $r_{\text{pin}} = 2$ is gradually switched on after $t = 94.25/e_F$ and switched off after stirring the superfluid n_{stir} times.

APPENDIX C: ENERGETICS

In Fig. 4 we compare how the total energy of the system changes through four sample stirring simulations. Both ETF and SLDA simulations with $v_{\text{stir}} \approx 0.1 v_F$ that result in a single vortex display the same qualitative behavior: First the energy increases as the stirring potential is turned on and fluid is displaced (slight quantitative differences on the 10% level appear here due to the aforementioned differences in the displaced densities). The stirring potential nucleates a vortex from the edge of the trap, and then effectively pins the vortex: the stirring potential displaces fluid, thereby creating an attraction for the vortex which also prefers a density depletion in its core. The vortex then oscillates in this pinning potential, causing an oscillating force on the stirring potential

that appears as oscillations in the energy $dE/dt = -\boldsymbol{F}\cdot\boldsymbol{v}$ as the stirring potential does work on the system. Since usually only one vortex is attached to the pinning site at any given time, the $\boldsymbol{F}$ can be associated with the pinning force exerted by the pinning potential on the vortex. Since the velocity of the stirrer, $\boldsymbol{v}$, is almost identical in the two simulations, this points to the fact that $\boldsymbol{F}$ (per unit length) is larger in the GPE compared to SLDA. This is not surprising because the force exerted on the superfluid by a potential V can be written as

$$\boldsymbol{F} = -\int d^2x\rho\nabla V, \tag{C1}$$

and the depletion in the density in the core of the vortex, which is the source of the pinning force, is smaller in the SLDA compared to the GPE.

Finally, the stirring potential is removed, leaving the single vortex, with an orbit determined by a countercirculating image vortex outside the trap [17]. The subsequent motion of the vortex is almost identical in both ETF and SLDA simulations since it results from long-distance superfluid hydrodynamic boundary effects rather than the buoyant force (the trap is flat at the orbital radius) which would be more sensitive to the difference in vortex mass due to nonzero occupation of the core in the SLDA.

For $v_{\text{stir}} \approx 0.2v_F$, a similar picture is presented: vortices are nucleated from the boundary of the system, and one remains pinned to the stirrer while three others perform complex orbits as governed by the Magnus relation in the presence of each other, the boundary of the trap, and the stirrer. The motions of the vortices appears to be chaotic—small changes in initial conditions, lattice resolution, etc., lead to different trajectories. For example, in the high-resolution 64^2 ETF simulation with $v_{\text{stir}} = 0.2v_F$, eventually four vortices remain in the bulk, whereas with the 32^2 simulation and the $v_{\text{stir}} = 0.197v_F$ simulations, one vortex attaches itself to the boundary of the trap and vanishes once the stirrer is removed, as in the corresponding SLDA simulation. At several times during the simulation, the stirring potential catches up with one of the free vortices and the vortex-pinning interaction exerts a stronger force on the stirrer, allowing it to perform work on this system; this appears as jumps in the energy evolution.

For $v_{\text{stir}} = 0.25v_F$, the ETF and the SLDA simulations have both qualitative and quantitative differences. The stirrer in the SLDA leaves five vortices in the bulk of the trap, while the 32^2 ETF simulation ends with only two vortices. Increasing the resolution to 64^2 gives six final vortices, though for a slightly smaller stirring speed ($v_{\text{stir}} = 0.242$) five vortices are left, matching SLDA. In the ETF, however, the stirrer creates

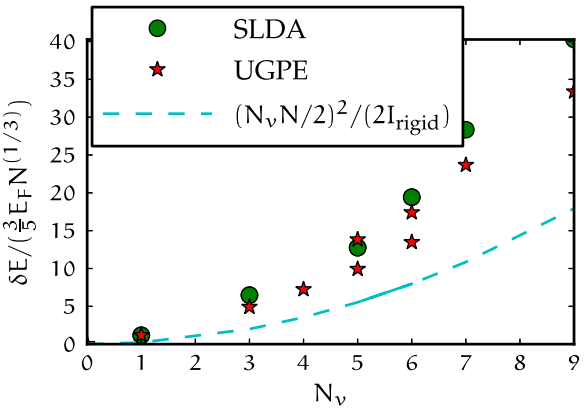

FIG. 9. (Color online) The excitation energy (the difference between the energy after the removal of the potential and before the introduction of the potential) as a function of the number of vortices created in the bulk (N_v).

filamentary structures that are not seen in the SLDA. For higher v_{stir}, the qualitative differences between the two models become even more pronounced; in particular, as discussed before, the low-resolution ETF simulations become so noisy that it is difficult to identify the vortices. With higher resolution, however, the ETF retains the somewhat striking property of the fermionic simulation, that coherent superfluidity persists for supersonic stirring $v_{\text{stir}} > c_s \approx 0.37v_F$. As pointed out in [14], this is due to the compressible nature of the superfluid: the stirring potential compresses the superfluid, raising the local critical velocity. Of course, strictly speaking, the ETF always remains superfluid, but for sufficiently fast stirring, the phase fluctuations are so rapid that a coarse-grained picture will find little spatial coherence. An improved two-fluid model would include such a coarse-graining procedure to convert superfluid to the normal fluid.

From the total energy difference after the stirrer is removed we can calculate the total excitation energy. This depends primarily on the number vortices added to the system, though there are minor contributions due to excited phonons. The classical estimate [14]

$$E_{\text{excit}} \sim L_z^2/(2I_{\text{rigid}}), \tag{C2}$$

where L_z is the angular momentum which is roughly proportional to the number of vortices, and I_{rigid} is the moment of inertia of the superfluid in the trap, suggests that it increases quadratically with the number of vortices. Equation (C2) is just a rough estimate, and it turns out to overestimate the excitation energy by a factor of 2, as we show in Fig. 9. The GPE provides a reasonable estimate of the excitation energy in the SLDA as a function of the number of vortices created, all the way up to $v_{\text{stir}} < v_F 0.35$.

[1] B. D. Josephson, Rev. Mod. Phys. **46**, 251 (1974).
[2] J. P. Park, P. Eames, D. M. Engebretson, J. Berezovsky, and P. A. Crowell, Phys. Rev. B **67**, 020403 (2003).
[3] X. Zhu, Z. Liu, V. Metlushko, P. Grütter, and M. R. Freeman, Phys. Rev. B **71**, 180408 (2005).
[4] S.-B. Choe, Y. Acremann, A. Scholl, A. Bauer, A. Doran, J. Stöhr, and H. A. Padmore, Science **304**, 420 (2004).
[5] R. L. Compton and P. A. Crowell, Phys. Rev. Lett. **97**, 137202 (2006).

[6] W. Ketterle and M. W. Zwierlein, Riv. Nuovo Cimento **31**, 247 (2008).

[7] I. Bloch, Nat. Phys. **1**, 23 (2005).

[8] U. Schneider, L. Hackermüller, J. P. Ronzheimer, S. Will, S. Braun, T. Best, I. Bloch, E. Demler, S. Mandt, D. Rasch, and A. Rosch, Nat. Phys. **8**, 213 (2012).

[9] J. A. Joseph, J. E. Thomas, M. Kulkarni, and A. G. Abanov, Phys. Rev. Lett. **106**, 150401 (2011).

[10] T. Yefsah, A. T. Sommer, M. J. H. Ku, L. W. Cheuk, W. Ji, W. S. Bakr, and M. W. Zwierlein, Nature (London) **499**, 426 (2013).

[11] I. Stetcu, A. Bulgac, P. Magierski, and K. J. Roche, Phys. Rev. C **84**, 051309(R) (2011).

[12] A. Bulgac, J. Phys. G **37**, 064006 (2010).

[13] B. Link, R. I. Epstein, and J. M. Lattimer, Phys. Rev. Lett. **83**, 3362 (1999).

[14] A. Bulgac, Y.-L. Luo, P. Magierski, K. J. Roche, and Y. Yu, Science **332**, 1288 (2011).

[15] A. Bulgac, M. M. Forbes, M. M. Kelley, K. J. Roche, and G. Wlazłowski, Phys. Rev. Lett. **112**, 025301 (2014).

[16] A. J. Fetter, arXiv:cond-mat/9811366.

[17] C. J. Pethick and H. Smith, *Bose-Einsten Condensation in Dilute Gases* (Cambridge University Press, Cambridge, 2002).

[18] W. Zwerger (ed.), *The BCS–BEC Crossover and the Unitary Fermi Gas*, Lecture Notes in Physics, Vol. 836 (Springer-Verlag, Berlin, 2012).

[19] J. Carlson, S. Gandolfi, and A. Gezerlis, Prog. Theor. Exp. Phys. **2012**, 01A209 (2012).

[20] The many-body challenge problem (MBX) was formulated by G. F. Bertsch in 1999. See also [73,74].

[21] J. Carlson, S.-Y. Chang, V. R. Pandharipande, and K. E. Schmidt, Phys. Rev. Lett. **91**, 050401 (2003).

[22] G. E. Astrakharchik, J. Boronat, J. Casulleras, and S. Giorgini, Phys. Rev. Lett. **93**, 200404 (2004).

[23] A. Bulgac, J. E. Drut, and P. Magierski, Int. J. Mod. Phys. B **20**, 5165 (2006).

[24] D. Lee, Phys. Rev. C **78**, 024001 (2008).

[25] M. M. Forbes, S. Gandolfi, and A. Gezerlis, Phys. Rev. Lett. **106**, 235303 (2011); Phys. Rev. A **86**, 053603 (2012).

[26] S. Nascimbène, N. Navon, K. J. Jiang, F. Chevy, and C. Salomon, Nature (London) **463**, 1057 (2010).

[27] M. Horikoshi, S. Nakajima, M. Ueda, and T. Mukaiyama, Science **327**, 442 (2010).

[28] M. J. H. Ku, A. T. Sommer, L. W. Cheuk, and M. W. Zwierlein, Science **335**, 563 (2012).

[29] M. G. Endres, D. B. Kaplan, J.-W. Lee, and A. N. Nicholson, Phys. Rev. A **87**, 023615 (2013).

[30] A. Bulgac and M. M. Forbes, in *Quantum Gases: Finite Temperature and Non-Equilibrium Dynamics*, Cold Atoms Series, Vol. 1, edited by N. P. Proukakis *et al.* (Imperial College Press, London, 2013), Chap. 26; A. Bulgac, M. M. Forbes, and P. Magierski, Chap. 9, pp. 305–373 of [18].

[31] W. Ketterle and M. W. Zwierlein, in *Ultra-cold Fermi Gases*, International School of Physics "Enrico Fermi", Vol. 164, edited by M. Inguscio, W. Ketterle, and C. Salomon (IOS Press, Amsterdam, 2007), pp. 95–287.

[32] A. Bulgac, M. M. Forbes, and R. Sharma, Phys. Rev. Lett. **110**, 241102 (2013).

[33] Y. E. Kim and A. L. Zubarev, Phys. Lett. A **327**, 397 (2004); Phys. Rev. A **70**, 033612 (2004).

[34] L. Salasnich, F. Ancilotto, N. Manini, and F. Toigo, Laser Phys. **19**, 636 (2009).

[35] L. Salasnich and F. Toigo, Phys. Rev. A **78**, 053626 (2008); **82**, 059902(E) (2010).

[36] Y. E. Kim and A. L. Zubarev, Phys. Rev. A **72**, 011603 (2005).

[37] Y. E. Kim and A. L. Zubarev, J. Phys. B **38**, 011603 (2005).

[38] L. Salasnich, F. Ancilotto, and F. Toigo, Laser Phys. Lett. **7**, 78 (2010); L. Salasnich, Few-Body Sys. **54**, 697 (2013).

[39] F. Ancilotto, L. Salasnich, and F. Toigo, Phys. Rev. A **85**, 063612 (2012); J. Low Temp. Phys. **171**, 329 (2013).

[40] F. Ancilotto, L. Salasnich, and F. Toigo, Phys. Rev. A **87**, 013637 (2013).

[41] S. Gautam, Mod. Phys. Lett. B **27**, 1350097 (2013).

[42] A. Khan and P. K. Panigrahi, J. Phys. B **46**, 115302 (2013).

[43] J. E. Drut, R. J. Furnstahl, and L. Platter, Prog. Part. Nucl. Phys. **64**, 120 (2010).

[44] P. Hohenberg and W. Kohn, Phys. Rev. **136**, B864 (1964).

[45] A. K. Rajagopal and J. Callaway, Phys. Rev. B **7**, 1912 (1973); V. Peuckert, J. Phys. C **11**, 4945 (1978); E. Runge and E. K. U. Gross, Phys. Rev. Lett. **52**, 997 (1984).

[46] A. Bulgac, Phys. Rev. C **65**, 051305(R) (2002); A. Bulgac and Y. Yu, Phys. Rev. Lett. **88**, 042504 (2002); M. M. Forbes, arXiv:1211.3779.

[47] W. Kohn and L. J. Sham, Phys. Rev. **140**, A1133 (1965).

[48] A. Bulgac, Phys. Rev. A **76**, 040502 (2007).

[49] M. Brack and R. K. Bhaduri, *Semiclassical Physics*, Frontiers in Physics, Vol. 96 (Addison-Wesley, Advanced Book Program, Reading, MA, 1997).

[50] C. F. v. Weizsäcker, Z. Phys. A **96**, 431 (1935).

[51] S. A. Khan and M. Bonitz, in *Complex Plasmas: Scientific Challenges and Technological Opportunities*, Springer Series on Atomic, Optical, and Plasma Physics, Vol. 82, edited by M. Bonitz, K. Becker, J. Lopez, and H. Thomsen (Springer, Berlin, 2014), Chap. XIII, p. 240.

[52] A. L. Zubarev, J. Phys. B **42**, 011001 (2009).

[53] L. Salasnich, Laser Phys. **19**, 642 (2009); S. K. Adhikari and L. Salasnich, New J. Phys. **11**, 023011 (2009).

[54] R. Combescot, M. Y. Kagan, and S. Stringari, Phys. Rev. A **74**, 042717 (2006).

[55] D. T. Son and M. B. Wingate, Ann. Phys. (NY) **321**, 197 (2006).

[56] A. Bulgac and Y. Yu, Phys. Rev. Lett. **91**, 190404 (2003).

[57] T. Busch, B.-G. Englert, K. Rzażewski, and M. Wilkens, Found. Phys. **28**, 549 (1998); T. Busch and J. R. Anglin, Phys. Rev. Lett. **84**, 2298 (2000).

[58] A. E. Muryshev, H. B. van Linden van den Heuvell, and G. V. Shlyapnikov, Phys. Rev. A **60**, R2665 (1999).

[59] P. O. Fedichev, A. E. Muryshev, and G. V. Shlyapnikov, Phys. Rev. A **60**, 3220 (1999).

[60] V. V. Konotop and L. Pitaevskii, Phys. Rev. Lett. **93**, 240403 (2004).

[61] C. Becker, S. Stellmer, P. Soltan-Panahi, S. Dorscher, M. Baumert, E.-M. Richter, J. Kronjager, K. Bongs, and K. Sengstock, Nat. Phys. **4**, 496 (2008); A. Weller, J. P. Ronzheimer, C. Gross, J. Esteve, M. K. Oberthaler, D. J. Frantzeskakis, G. Theocharis, and P. G. Kevrekidis, Phys. Rev. Lett. **101**, 130401 (2008).

[62] R. G. Scott, F. Dalfovo, L. P. Pitaevskii, and S. Stringari, Phys. Rev. Lett. **106**, 185301 (2011).

[63] R. G. Scott (private communication).
[64] S. Simonucci, P. Pieri, and G. C. Strinati, Phys. Rev. B **87**, 214507 (2013).
[65] G. Giuliani and G. Vignale, *Quantum Theory of the Electron Liquid* (Cambridge University Press, Cambridge, 2005).
[66] L. Juan Mañes and M. A. Valle, Ann. Phys. (NY) **324**, 1136 (2009); A. M. J. Schakel, *ibid.* **326**, 193 (2011).
[67] G. Rupak and T. Schaefer, Nucl. Phys. A **816**, 52 (2009).
[68] C. W. Gardiner, J. R. Anglin, and T. I. A. Fudge, J. Phys. B **35**, 1555 (2002).
[69] W. Wan, S. Jia, and J. W. Fleischer, Nat. Phys. **3**, 46 (2007); S. J. Rooney, P. B. Blakie, and A. S. Bradley, Phys. Rev. A **86**, 053634 (2012).
[70] M. J. Davis, S. A. Morgan, and K. Burnett, Phys. Rev. Lett. **87**, 160402 (2001).
[71] R. W. Hamming, *Numerical Methods for Scientists and Engineers* (McGraw-Hill, Inc., New York, 1973).
[72] J. Huyghebaert and H. D. Raedt, J. Phys. A **23**, 5777 (1990).
[73] G. A. Baker, Jr., Phys. Rev. C **60**, 054311 (1999).
[74] G. A. Baker, Jr., Int. J. Mod. Phys. B **15**, 1314 (2001).